

## CO OBSERVATIONS OF SEVERAL GALACTIC H II REGIONS

F. P. ISRAEL<sup>a1</sup>Owens Valley Radio Observatory, California Institute of Technology, Pasadena, California 91125  
and Goddard Institute for Space Studies, New York, New York 10025*Received 14 December 1979; revised 6 August 1980*

## ABSTRACT

Maps of the CO emission at a resolution of 8 arcmin are presented for seven H II regions or H II region groups; the results of a search for CO emission near seven more are also given. CO was detected near all but two of the observed objects. The distribution of <sup>12</sup>CO and <sup>13</sup>CO near S142, S157, and S159 was mapped at a resolution of 2.3 arcmin. The S147/S153 group of H II regions is shown to consist of physically related objects; it is a region of active star formation. The results show a complicated molecular cloud structure near most observed H II regions. There is a tendency for decreasing CO cloud mass when H II regions in more evolved stages are observed. The relevance of these results for the understanding of individual H II region/molecular cloud complexes, and for general aspects of the star-formation process, is briefly discussed.

## I. INTRODUCTION

Several galactic surveys of the <sup>12</sup>CO ( $J = 1 \rightarrow 0$ ) line have established a close relationship between CO clouds and H II regions (cf. Liszt 1973, Wilson *et al.* 1974, and Blair *et al.* 1975). This relationship was further interpreted by Israel (1978) in terms of a blister picture: OB stars form at the edge of molecular clouds and subsequently ionize the parts of the clouds nearest to them. In doing so they send an ionization front into the molecular cloud with velocities of 2–3 km s<sup>-1</sup>. Ionized matter streams away from these ionization fronts with speeds of the order of 10–20 km s<sup>-1</sup>. This picture is consistent with the detailed results of CO mapping of large and bright H II region complexes, such as, for instance, W49 (Mufson and Liszt 1977), W75/DR 21 (Cong 1977; Dickel *et al.* 1978), and W3 (Lada *et al.* 1978b; Dickel *et al.* 1980), and large evolved H II regions such as M17 (Lada 1976; Elmegreen *et al.* 1979) and the North America Nebula (Bally and Scoville 1980).

The CO distribution near optically visible, small H II regions has rarely been mapped. Notable exceptions are S106 (Lucas *et al.* 1978), S228 (Lucas and Encenaz 1975), S252 (Baran 1978; Lada and Wooden 1979), S255 (Evans *et al.* 1977), and S140 (Blair *et al.* 1978). Yet these H II regions offer, because of their relative simplicity, the best opportunities for studying detailed relationships between ionized regions and neutral clouds. For this reason I observed CO emission in the direction of several small Sharpless (1959) H II regions. The results for the W58 group (K3-50, ON-3, S99, and S100) have been discussed elsewhere (Israel 1980). In this paper, I present detailed observations of four molecular

clouds near seven H II regions or groups of H II regions (Blitz 1, S125, S142, S147/S153, S157, S159, and S206), and some additional results for seven more H II regions.

## II. OBSERVATIONS

All observations described in this paper were made in March 1976 (at Columbia University) and April 1976 [at the Millimeter Wave Observatory (MWO) in Texas\*].

First, <sup>12</sup>CO emission was observed with the Columbia University 1.2-m telescope in New York City. This telescope has a full beamwidth at half power of 8 arcmin and a beam efficiency of 70% at the frequency of the  $J = 1 \rightarrow 0$  transition of <sup>12</sup>CO (115 GHz). At the time of observation, the receiver had a single-sideband noise temperature of 1500 K. The spectrometer consisted of a filter bank with a total bandwidth of 40 MHz and a spectral resolution of 1 MHz (corresponding to 2.6 km s<sup>-1</sup> at 115 GHz). Since the observations were made by frequency switching over an interval of 20 MHz, the velocity range used was 52 km s<sup>-1</sup>. The integration time per point was 3 min; several positions were observed more than once in order to check the system stability and the data quality.

Three objects were mapped at higher resolution, and in both <sup>12</sup>CO and <sup>13</sup>CO with the MWO 5-m telescope. This telescope has a half-power beamwidth of 2.3 arcmin and a beam efficiency of 85% at 115 GHz. The receiver had a single-sideband noise temperature varying from

\* The Millimeter Wave Observatory at Fort Davis, Texas is operated by the Electrical Engineering Research Laboratory, University of Texas at Austin, with support from the National Science Foundation and McDonald Observatory.

<sup>a1</sup> Present address: Estec, SSD, Postbus 229, 2200 AG, Noordwyk, The Netherlands.

TABLE I.  $^{12}\text{CO}$  cloud parameters (Columbia observations).

Cloud	Peak position		Peak $T_A$ (K)	$V_{\text{LSR}}$ ( $\text{km s}^{-1}$ )	FWHM $\Delta V$ ( $\text{km s}^{-1}$ )	Assumed distance (kpc)	Size		Associated H II region
	$\alpha$ (1950)	$\delta$ (1950)					(arcmin)	(pc)	
CO90.2-2.3	21 <sup>h</sup> 21 <sup>m</sup> 0	+46°40'	2.9	+1.5	2.6	1.0	~10	<3	Blitz 1
CO94.4-5.4	21 51.2	+47 09	5.0	+8.1	3.1	1.0	16	5	S125
CO93.7-4.4	21 44.0	+47 25	[5.0]	+2.9	—	1.0	—	—	—
CO107.2-0.9	22 46.2	+57 49	1.7	-41.2	2.6	4.0	4 × 8	6	S142
CO108.3-1.1	22 54.0	+58 14	3.7	-54.0	5.2	4.5	11 × 23	16	S147, 148, 149
CO108.7-0.8	22 56.0	+58 34	5.2	-51.0	2.9	4.5	21 × 29	25	S152, 153
CO109.1-0.4	22 56.0	+59 10	5.3	-49.0	3.4	4.5	12 × 23	16	—
CO111.0-1.0	23 13.0	+59 24	1.9	-44.5	23	3.5	7 × 20	12	S157
CO123.1-6.3	00 49.5	+56 20	2.2	-30.5	5.4	2.1	15 × 35	13	S184
CO150.5-0.8	03 59.6	+51 19	3.3	-24.3	5.5	3.7	14 × 29	22	S206
CO150.8-1.0	04 00.5	+51 03	1.9	-34.5	5.0	3.7	12	13	S206
CO151.2-0.4	04 04.7	+51 11	1.8	-26.9	4.2	—	10 × 12	—	—
CO151.2-1.0	04 02.2	+50 47	1.6	-11.3	7.0	—	10	—	—
CO151.2-1.2	04 02.3	+50 39	2.5	-32.3	4.7	3.7	12 × 25	19	—

1500 to 2000 K. The filter bank had a total bandwidth of 10 MHz and a resolution of 250 kHz (corresponding to  $0.65 \text{ km s}^{-1}$  at 115 GHz). Again all observations were made by frequency switching over an interval of 5 MHz; the integration time per point was 5 min. For both telescopes, the receivers were calibrated against an ambient temperature load by a chopperwheel technique (cf. Davis and VandenBout 1973). In the case of the observations in New York City, an additional atmospheric correction was applied in order to take into account the different scale heights of atmospheric water vapor and oxygen.

### III. RESULTS AND ANALYSIS

#### a) General Results

The observational results are summarized in Tables I-III.

Table I gives the results of the mapping program carried out with the Columbia University 1.2-m dish at 8-arcmin resolution. All CO clouds found, and the associated H II regions, are listed. Table II gives the results obtained with the same telescope, for the detected molecular clouds that were not mapped. Because of the limited resolution in space and in velocity, it was not always possible to separate different components. Therefore, in both tables the value given for  $\Delta V$  indicates the full range over which  $^{12}\text{CO}$  emission is seen—high values thus may indicate the presence of multiple velocity

components rather than single, wide lines. This is certainly the case for S157, as a comparison with Table III will show. Table III lists the results obtained with the MWO 5-m telescope at a resolution of 2.3 arcmin. The  $^{13}\text{CO}$  column densities were calculated under the usual LTE assumptions. Molecular hydrogen space densities were derived assuming  $N(\text{H}_2) = 5 \times 10^5 N(^{13}\text{CO})$  (Dickman 1978) and assuming a line-of-sight dimension equal to the mean diameter of each cloud. In the following, I will discuss the observations in more detail.

#### b) S125 (IC 5146) and Blitz 1

The H II region S125 is of some interest since it is associated with the very young cluster IC 5146 (Walker 1959). It was mapped at high resolution by Israel (1977b); it is rather featureless and appears to be excited by an early B star. Riegel (1967) found S125 to be associated with an H I cloud with a size of about 23 arcmin, an FWHM velocity width of  $6 \text{ km s}^{-1}$ , and a calculated mass of  $670 M_{\odot}$ . The present CO results, obtained with a beam size comparable to the one used for the H I observations, are shown in Figs. 1. Figure 1(a) shows the distribution of CO on the sky, integrated over the full observed velocity range. Near S125, a clear CO maximum with a size of about 15 arcmin and an FWHM of  $3 \text{ km s}^{-1}$  is seen at the same position as the H I cloud. The CO velocity seems to be higher than the H I velocity by

TABLE II.  $^{12}\text{CO}$  emission near galactic H II regions (Columbia observations).

H II region	CO position		$T_A$ (K)	$V_{\text{LSR}}$ ( $\text{km s}^{-1}$ )	FWHM $\Delta V$ ( $\text{km s}^{-1}$ )	Number of positions measured	H II region $V_{\text{LSR}}$ ( $\text{km s}^{-1}$ )	Position difference (arcmin)
	$\alpha$ (1950)	$\delta$ (1950)						
S188	01 <sup>h</sup> 28 <sup>m</sup> 3	+57°59'	0.7	-16.0	10	4	-14.5	11
S195	02 39.0	+59 24	1.2	-16.0	4	18	—	8
	02 38.0	+59 40	1.2	0.0	3			17
S196	02 46.9	+62 20	1.4	-60.0	9	4	-43.0	16
S266	06 16.5	+15 19	1.4	+5.0	17	2	—	6
S269	06 11.4	+13 51	1.1	+19.0	7	1	+12.0	6
S271	06 12.1	+12 22	1.5	+21.0	4	4	+16.6	0

TABLE III. CO cloud parameters (MWC observations).

Cloud	Peak position		$V_{\text{LSR}}$ ( $\text{km s}^{-1}$ )	Peak	Peak	FWHM	Assumed (arc- distance)	Size (arc- min)	Size (pc)	Peak $N(^{13}\text{CO})$ ( $\text{cm}^{-2}$ )	$n(\text{H}_2)$ ( $\text{cm}^{-3}$ )	Mass ( $M_{\odot}$ )
	$\alpha$ (1950)	$\delta$ (1950)		$T_A^*$ ( $^{12}\text{CO}$ ) (K)	$T_A^*$ ( $^{13}\text{CO}$ ) (K)	$\Delta V$ ( $^{13}\text{CO}$ ) ( $\text{km s}^{-1}$ )						
S142:												
CO107.2-0.9	22 <sup>h</sup> 46 <sup>m</sup> 00	+57°51'40"	-42.8	5.0	<0.3	2.7 <sup>a</sup>	2	4.0	2	<0.7	<60	<15
CO107.3-0.9	22 46 15	+57 55 00	-41.1	3.0 <sup>b</sup>	1.0	1.5	3		3	1.8	100	80
S157:												
CO111.2-0.6	23 13 00	+59 45 00	-48.6	8.7	—	—	~2	3.5	~2	—	—	—
CO111.2-0.7	23 13 00	+59 40 20	-44.7	7.2	—	—	3 × 5		4	—	—	—
CO111.3-0.7 <sup>c</sup>	23 14 00	+59 45 30	-43.0	14.6	4.9	2.6	8 × 3		5	18.5	10 <sup>15</sup> 600-100	2600
CO111.3-0.9	23 15 00	+59 33 00	-46.0	5.2	—	—	5 × <2		3	—	—	—
CO111.4-0.5	23 14 40	+59 55 12	-48.0	13.2	3.5	2.2	6 × 7		6	10.1	300	2650
CO111.4-0.7	23 15 00	+59 48 00	-43.4	6.5	1.8	1.0	5 × 2		3	1.9	100-150	110
CO111.5-0.7	23 15 40	+59 50 30	-46.6	3.6	—	—	<2		<2	—	—	—
S159:												
CO111.6+0.4 <sup>d</sup>	23 13 10	+60 50 30	-56.3	15.6	5.2	2.9	5	3.5	5	22.7	750	3600
CO111.8+0.4	23 14 50	+60 54 45	-54.3	12.0	3.2 <sup>b</sup>	3.1 <sup>b</sup>	7		7	12.2 <sup>b</sup>	280-500	3350

<sup>a</sup>  $^{12}\text{CO}$  halfwidth.

<sup>b</sup>  $^{13}\text{CO}$  parameters are not at  $^{12}\text{CO}$  peak position, but one beamwidth to the southwest.

<sup>c</sup> Associated with S157A, B.

<sup>d</sup> Associated with S159A.

about  $1 \text{ km s}^{-1}$  (see also Milman *et al.* 1975 and Lada and Elmegreen 1979). With a diameter of about 10 arcmin, the H II region in turn has a size comparable to, but smaller than, the CO and the H I clouds. An upper limit to the ionized mass is only  $7M_{\odot}$  (Israel 1977b).

Observations with the MWO at 2.3-arcmin resolution (Lada and Elmegreen 1979) show the CO to be distributed mainly in the form of three lobes around the ionized region, with a mean  $^{13}\text{CO}$  column density of  $1 \times 10^{16} \text{ cm}^{-2}$ . Together with the total size of 16 arcmin (Table I) this yields an estimated neutral mass of about  $M(\text{H}_2) = 1350M_{\odot}$ , twice as high as the value  $M(\text{H}_2) = 630M_{\odot}$  calculated by Lada and Elmegreen (1979) for the dense lobes alone. A more realistic value for the neutral mass is probably somewhere in between these two: I will adopt  $M(\text{H}_2) = 1 \times 10^3 M_{\odot}$ . Lada and Elmegreen (1979) discuss in some detail aspects of the star-formation process in S125; among other things they conclude that S125 is an evolved H II region that is beginning to disrupt the molecular cloud. The seeming lack of high-density regions in the ionized zone (Israel 1977b) supports the idea of S125 being an evolved object. If the CO can be considered to represent the high-density interface between the ionized region and the H I cloud, then, at least locally, star formation cannot proceed for very long into the future, given the limited amounts of mass available in the form of atomic and molecular hydrogen. Elias (1978) mapped roughly the same region as depicted in Fig. 1(a) at a wavelength of  $2.2 \mu\text{m}$ . He found an FU Orionis star embedded in the dark cloud at R.A. =  $21^{\text{h}}45^{\text{m}}27^{\text{s}}$ , Decl. =  $47^{\circ}18'$ ; he did not find any new heating sources at  $2 \mu\text{m}$ .

The CO maximum lies at the eastern tip of a much larger, very elongated molecular cloud that is easily seen on Palomar Sky Survey prints. Three of the four CO measurements by Milman *et al.* (1975) are of this elongated cloud. At the maximum CO antenna temperature mapped in Fig. 1(a), this CO cloud has a  $V_{\text{LSR}}$

=  $3 \text{ km s}^{-1}$ , lower by about  $5 \text{ km s}^{-1}$  than the velocity of the compact CO cloud associated with S125 [Fig. 1(b)]. Nevertheless, the two are indeed connected by a low surface brightness bridge of molecular material [Fig. 1(c)]. Thus a gradient of  $5 \text{ km s}^{-1}$  is present over an angular distance of 70 arcmin, corresponding to a projected linear gradient of  $0.25 \text{ km s}^{-1} \text{ pc}^{-1}$ . The data by Milman *et al.* (1975) indicate that this gradient continues eastward for at least half a degree more.

The object Blitz 1 was discovered by Blitz (private communication). A compact CO cloud is located in a dusty region southwest of the filamentary molecular cloud discussed above. Most probably the object is likewise at a distance of about 1 kpc. The integrated  $^{12}\text{CO}$  emission shows a clear maximum, but the position-velocity diagram indicates that this is caused by the superposition of two different components (Figs. 2). The CO cloud is not fully mapped, and suggests the appearance of a very narrow ridge.

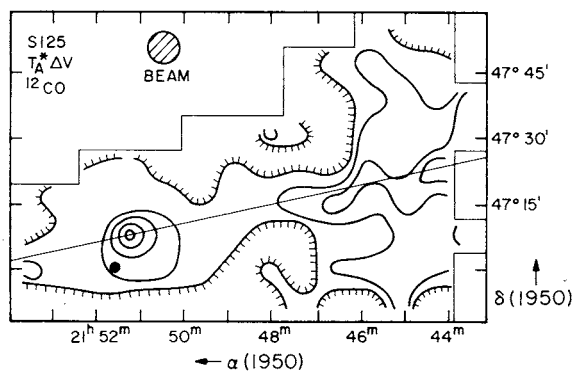


FIG. 1(a).  $^{12}\text{CO}$  map of S125 (IC 5146) integrated over a velocity range of  $V_{\text{LSR}} = +31 \text{ km s}^{-1}$  to  $V_{\text{LSR}} = -18 \text{ km s}^{-1}$ . LSR contour values are in steps of  $3.9 \text{ K km s}^{-1}$ . Contour values are in steps of  $3.9 \text{ K km s}^{-1}$ .

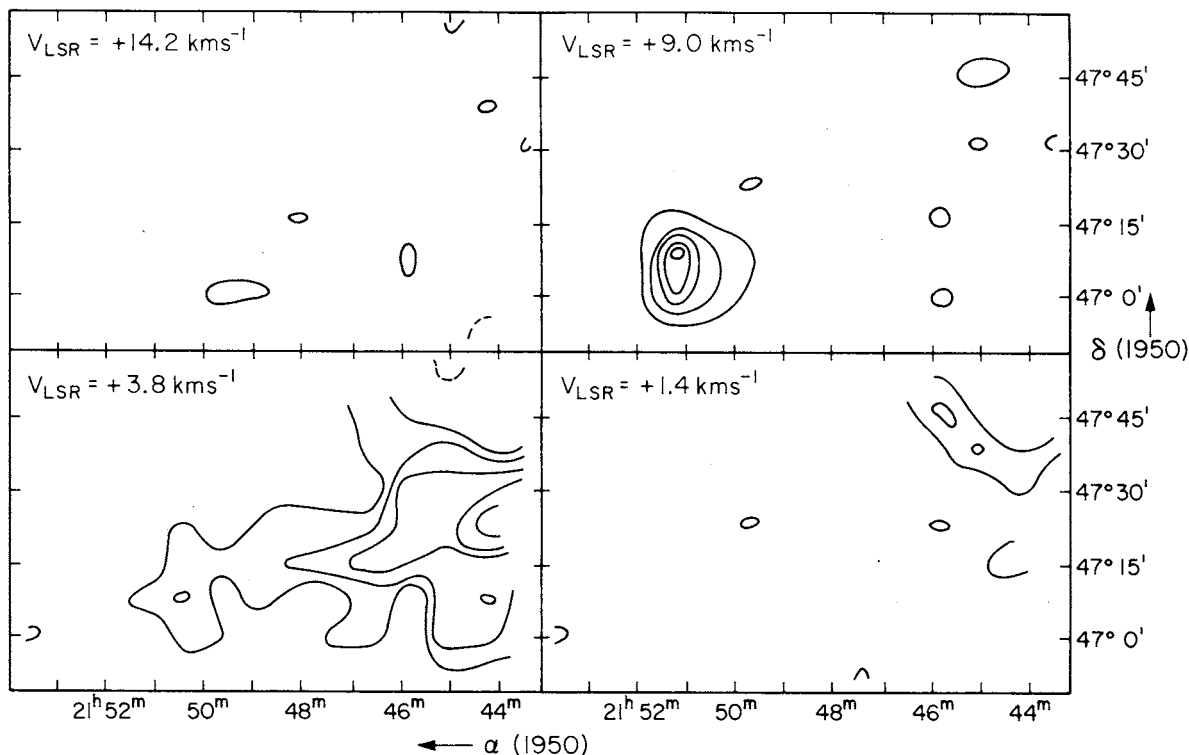


FIG. 1(b).  $^{12}\text{CO}$  maps at different velocities, integrated over two channels. Contour values are in steps of  $2.6 \text{ K km s}^{-1}$ .

c) S142 (NGC 7380)

The H II region S142 has all the trappings of a large evolved emission nebula (Israel 1977b). The H II region shows some structure in its northeast corner, where minor density fluctuations in the ionized gas correlate with bright rim structures in optical pictures (Israel 1977b). It is at this rather eccentric position that a small and weak CO cloud is found [Table I and Fig. 3(a)]. The brightest part of the CO cloud is adjacent to the bright rim structures, and the wider envelope seems to be largely behind the nebula. The core was mapped in more detail with the MWO telescope [Figs. 3(b) and 3(c)]. A

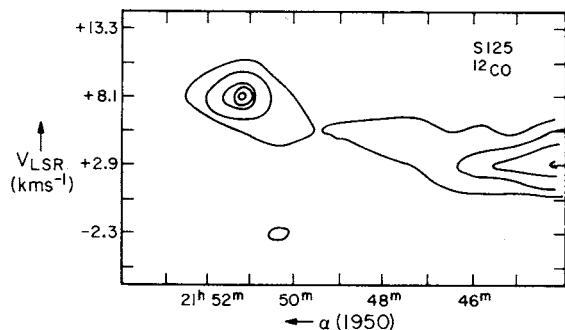


FIG. 1(c).  $^{12}\text{CO}$  position-velocity map along the line marked in Fig. 1(a). Contour values are in steps of  $1.0 \text{ K}$ .

comparison of the  $^{12}\text{CO}$  and  $^{13}\text{CO}$  maps shows that this core, which coincides with an obscuring region on the Palomar Sky Survey prints, consists of two components: a dense [relatively high  $T_A^*$  ( $^{13}\text{CO}$ )] component at  $V_{\text{LSR}} = -41.1 \text{ km s}^{-1}$  [see also Fig. 3(d)] and a hot [relatively high  $T_A^*$  ( $^{12}\text{CO}$ )] component at  $V_{\text{LSR}} = -42.8 \text{ km s}^{-1}$ . The hot component is unresolved by the 2.3-arcmin MWO beam. The mass of the high-density component is low:  $M(\text{H}_2) = 80 M_{\odot}$ . The lower-density envelope may

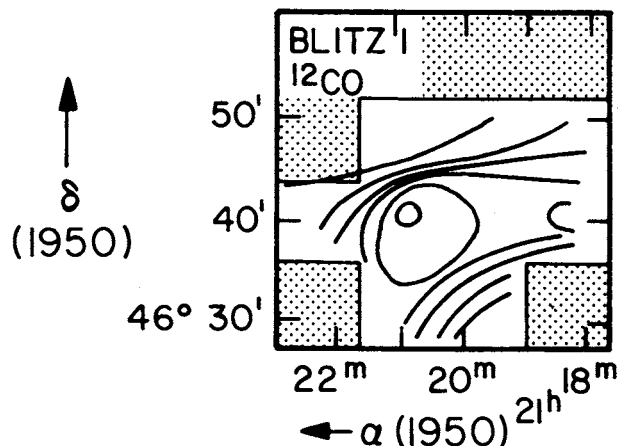


FIG. 2(a).  $^{12}\text{CO}$  map of Blitz 1 integrated over a velocity range  $V_{\text{LSR}} = +31$  to  $-18 \text{ km s}^{-1}$ . Contour values are in steps of  $2.6 \text{ K km s}^{-1}$ .

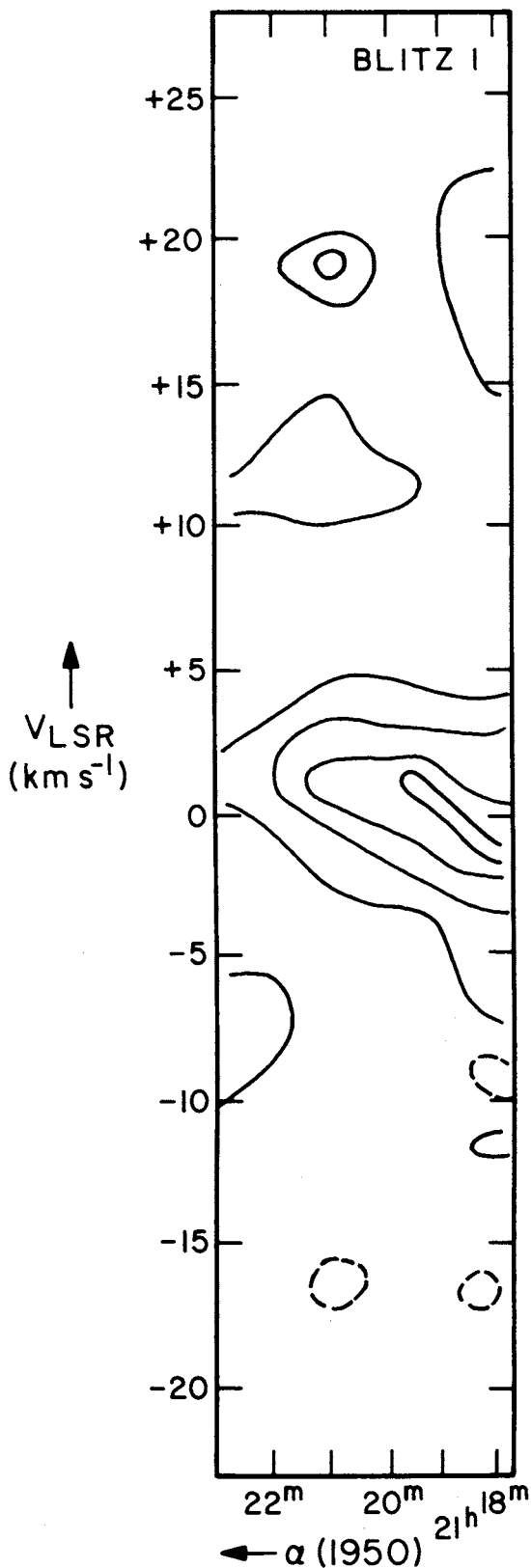


FIG. 2(b).  $^{12}\text{CO}$  position-velocity map at constant declination (Decl. =  $46^{\circ}40'$ ). Contour values are in steps of 1.0 K; the 0.5-K contour is also given.

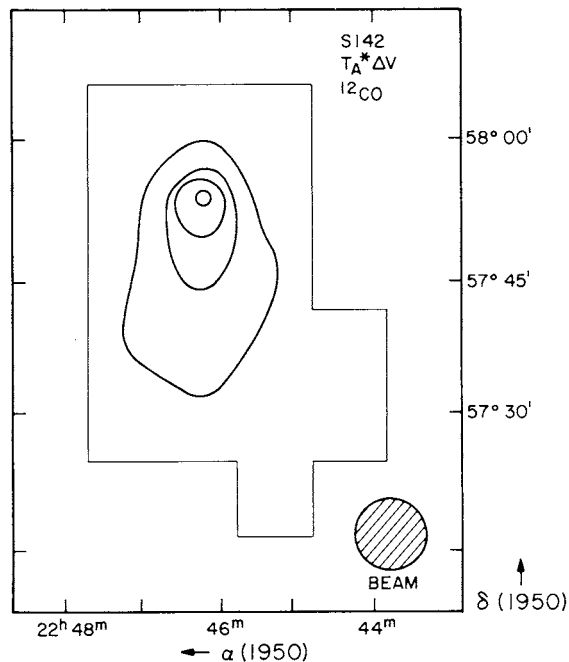


FIG. 3(a).  $^{12}\text{CO}$  map of S142 (NGC 7380) integrated over a velocity range  $V_{\text{LSR}} = -10$  to  $-59 \text{ km s}^{-1}$ . Contour values are in steps of  $2.6 \text{ K km s}^{-1}$ .

contribute as much again, so that the total neutral mass is of order  $(150\text{--}200)M_{\odot}$ . The case of S142 is interesting in several respects. With its mean size of 6 arcmin (7 pc), the CO cloud is quite a bit smaller than the H II region with which it is associated (12 arcmin or 14 pc)—a situation contrary to that commonly observed. The nebula S142 is excited by stars that are part of the young open cluster (age  $2 \times 10^6$  yr, Moffat 1971) NGC 7380; this cluster contains at least four early-type OB stars, among which is the O6 double DH Cep. The positions of three of these stars is marked in Figure 14 of Israel (1977b), but see also Figure 5 of Moffat (1971). The fourth star, LS II  $57^{\circ}83$  is surrounded by a small knot of H II emission. The cluster center is offset from the nebula by about 6 arcmin (7 pc) in a northern direction. I suggest that the following scenario applies: Several million years ago, the bulk of the cluster was formed; the center of activity was about 10–15 pc to the northwest of the nebula. Since the exciting stars tend to be found in the southern part of the cluster, there is some evidence that these formed last, or at least interrupted further star formation in this direction. The rather dispersed early-type stars created small ionized regions that subsequently expanded and merged to form the present nebula S142. As the nebula further expanded, it ran into a nearby neutral cloud, which was then compressed and ionized from the outside (hence the bright rim structure), in particular by the O9 star LS II  $57^{\circ}90$ . It is therefore doubtful whether the CO cloud associated with S142 can be considered a remnant of the initial burst of star formation. Given this picture, it is a

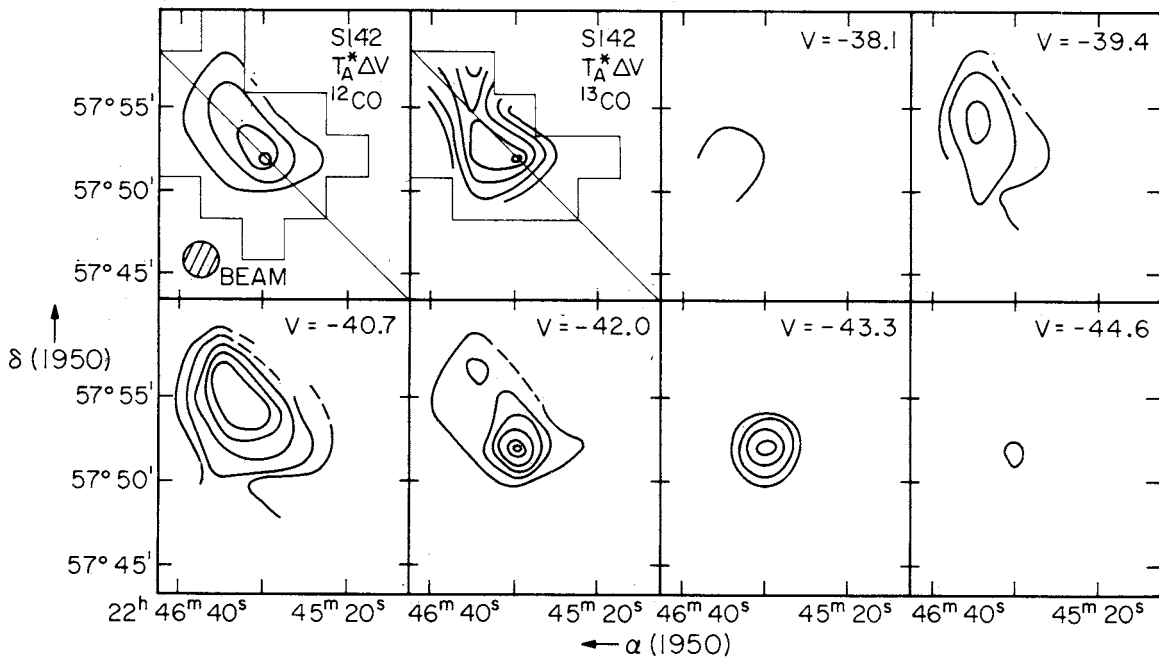


FIG. 3(b).  $^{12}\text{CO}$  and  $^{13}\text{CO}$  maps of S142. The two left most maps in the upper row are integrated over a velocity range  $V_{\text{LSR}} = -35.5$  to  $-48.5$   $\text{km s}^{-1}$ . Contour values are in steps of  $1 \text{ K km s}^{-1}$  for the  $^{13}\text{CO}$  map. The remaining six maps are  $^{12}\text{CO}$  channel maps integrated over two channels. Contour values are in steps of  $0.2 \text{ K km s}^{-1}$ .

matter of great interest to determine whether the interaction of S142 with the molecular cloud has led to further secondary activity, as envisioned in models of sequential star formation. Clearly, no compact H II region is present with  $S(21 \text{ cm}) \geq 10 \text{ mJy}$ ; neither are there any

known OH/ $\text{H}_2\text{O}$  masers. However, the hot compact CO source may be either an externally heated globule in the process of disintegration, or an internally heated object. Thus, infrared observations of this object might be of value. In any case, the low mass of the molecular cloud (at best  $200 M_{\odot}$ ) indicates that star formation, if taking place at all, is probably limited to at most a few stars of relatively low mass. Thus, S142/NGC 7380 seems to be representative of the last stages of star formation that started a few million years ago and has led to the birth of a moderately rich open cluster.

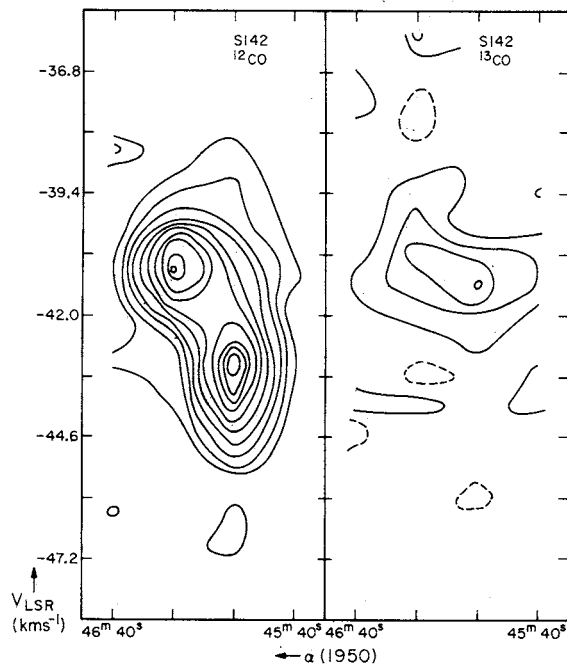


FIG. 3(c). Position-velocity maps in  $^{12}\text{CO}$  and  $^{13}\text{CO}$  along the line marked in Fig. 3(b). Contour values are in steps of  $1 \text{ K}$  for  $^{12}\text{CO}$  and  $0.5 \text{ K}$  for  $^{13}\text{CO}$ .

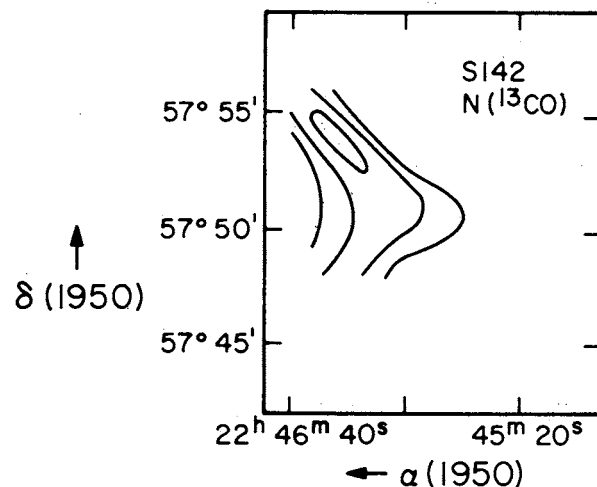


FIG. 3(d). Map of  $^{13}\text{CO}$  column densities in S142. Contours are in steps of  $1.5 \times 10^{15} \text{ cm}^{-2}$ .

#### d) The S147/S153 Group

About 1.5 deg east of S142 (100 pc at a distance of 4 kpc), two groups of small H II regions are found.\* The first group consists of the faint H II region S147, and the bright and compact objects S148 and S149 (M1-20). On the basis of their H $\alpha$  radial velocities (Georgelin 1975), their distance is about 4.5 kpc, which places them, like S142, in the Perseus Arm. The second group consists of the bright and compact object S152 (M1-21) and the more extended and diffuse S153. Relatively little is known about most of them; however, S149 and S152 have been included in several surveys. Both are associated with a near-infrared source (Bergeat *et al.* 1975; Frogel and Persson 1972; Price and Walker 1976).†

Near S152/S153 the obscured infrared source AFGL 2999 is found (Price and Walker 1976). At the same position, Lo *et al.* (1975) found an H<sub>2</sub>O maser; this object is therefore most likely a young, compact H II region. The radio properties of S148 and S152 (Israel 1977c; Felli *et al.* 1978) indicate electron densities of the order of 500–1000 cm<sup>-3</sup> and emission measures of  $3 \times 10^5$  pc cm<sup>-6</sup>, likewise classifying them as fairly young objects. Radio maps of both sources show dense, elongated structures that are probably ionization fronts (cf. Israel 1977c). Thus, there is little doubt that both groups mark regions of recent or ongoing star formation. At the position of these H II regions, I found a large, elongated CO complex with a length of at least 1.8 deg, corresponding to linear dimensions of 130 pc or more [Figs. 4(a) and 4(b)].

In the south, the cloud may extend beyond the map boundary in a western direction. The complex contains three clear maxima, each with typical dimensions of 15–20 pc (cf. Table I). Figures 4(a) and 4(b) show the pair S148/S149 to be very close to the southernmost CO maximum; it has  $\Delta V(\text{H}\alpha\text{-CO}) = -4$  km s<sup>-1</sup>. The obscured source AFGL 2999/H<sub>2</sub>O is close to the central maximum and has about the same velocity. Both S152 and S153 are about a beamwidth (8 arcmin or 10 pc) east of the central peak, but CO observations by Dickinson *et al.* (1974) with the Kitt Peak 1.1-arcmin beam show a local CO peak just south of S152. It is clear, therefore, that the three maxima probably contain appreciable small-scale structure not seen by the large Columbia beam. S152 and S153 have  $V(\text{H II-CO}) = 0$  and  $-6$  km s<sup>-1</sup>, respectively. The results for S148/S149, AFGL 2999/H<sub>2</sub>O, S152, and S153 are therefore in agreement with the blister model (Israel 1978).

No H II region or maser source is known at the position of the northernmost CO maximum; a search for mid-infrared (10- $\mu$ m) sources at intermediate sensitivity levels (2–3 Jy) yielded negative results (Nadeau, private communication).

\* For a reproduction of the red PSS prints, showing the Perseus Arm from S142 to S159, see Israel *et al.* (1973), Figure 1.

† Since S148 and S149 are less than 2 arcmin apart, it is not clear to which object the AFGL observations apply.

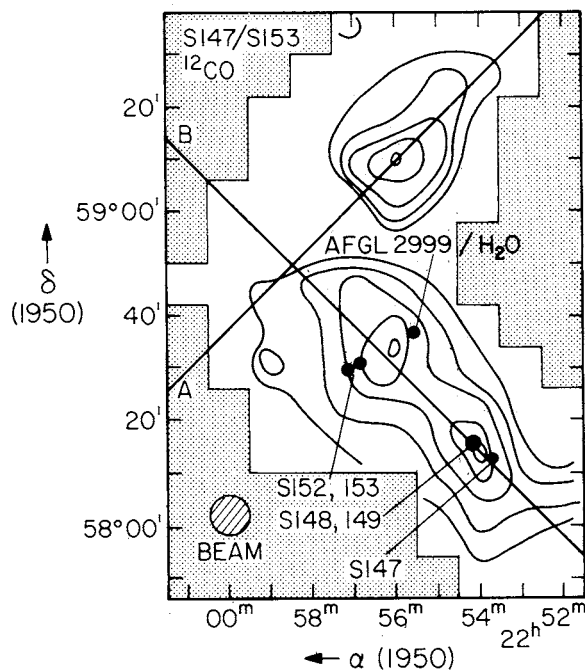


FIG. 4(a). <sup>12</sup>CO map of the S147/S153 cloud, integrated over a velocity range  $V_{\text{LSR}} = -28$  to  $-77$  km s<sup>-1</sup>. Contour values are in steps of 5.2 K km s<sup>-1</sup>.

The position-velocity maps of the cloud complex [Fig. 4(b)] show velocities in the range  $V_{\text{LSR}} = -47$  to  $-60$  km s<sup>-1</sup>. The northern cloud has a velocity gradient of 5 km s<sup>-1</sup> over 30 arcmin (35 pc), whereas the southern and central clouds have velocities that differ only slightly; in fact, their velocity structure is suggestive of a ring with its highest density at the far side, and expanding with a velocity of 5–8 km s<sup>-1</sup>. At the same velocity, the Green Bank–Maryland Survey shows an elongated H I complex, about 3 deg (225 pc) long (Westerhout 1969). The present CO cloud coincides with a hole in this complex. Although the southwestern extension points roughly in the direction of S142, it is unlikely that the S147/S153 cloud complex is connected to the CO cloud near S142. The latter has a velocity of  $V_{\text{LSR}} = -42$  km s<sup>-1</sup>, different by more than 10 km s<sup>-1</sup> from the southern S147/S149 CO cloud.

Summarizing, we have seen that the S147/S153 consists of a group of young H II regions that are close in space (within 35 pc of each other), and that are associated with a sizable amount of dense neutral matter. At present, it contains at least six young OB stars, and star formation is still taking place.

#### e) Central Part of S157

S157 is a large H II region of peculiar form, located at a distance of 3.5 kpc in the Perseus Arm. Part of the nebula was studied at radio wavelengths by Israel (1977c), in particular the compact H II regions S157A

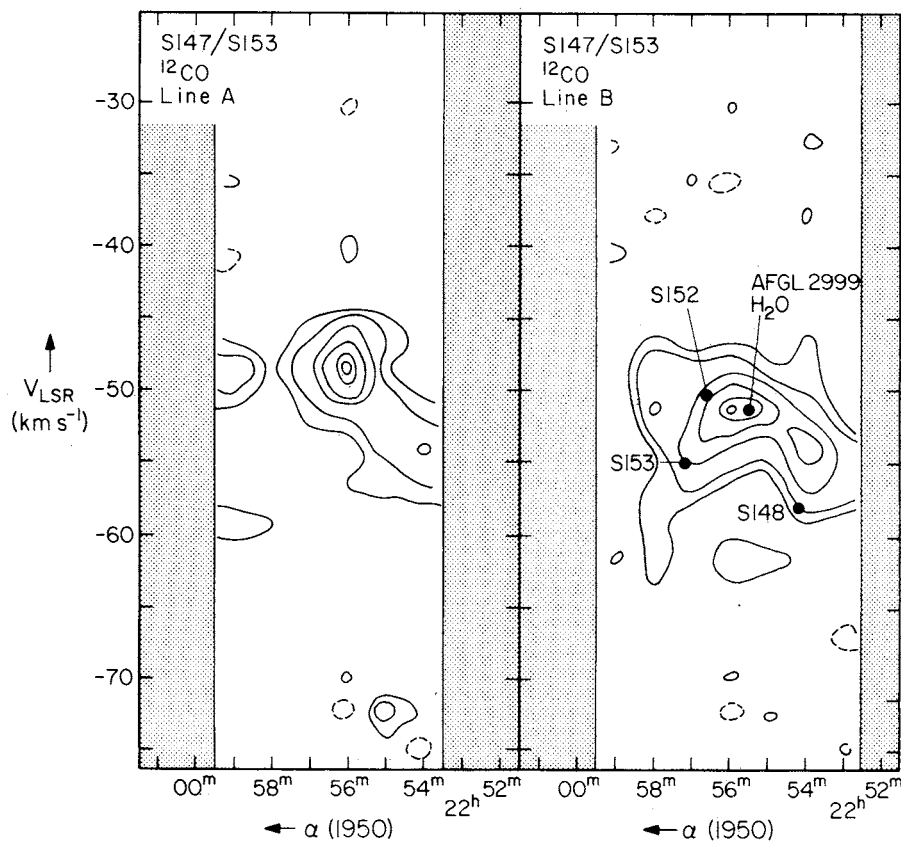


FIG. 4(b). Position-velocity maps in  $^{12}\text{CO}$ , along the lines marked in Fig. 4(a). Contour values are in steps of 1 K; the 0.5-K contour is also given.

and B in the central part of S157. The structure of the molecular cloud complex associated with S157 is complicated. In the small area mapped with the MWO

telescope (roughly 25 or 30 arcmin), at least seven individual clouds are visible over a velocity range of about  $10 \text{ km s}^{-1}$  [see Figs. 5(a)-5(c) and Table III]. The

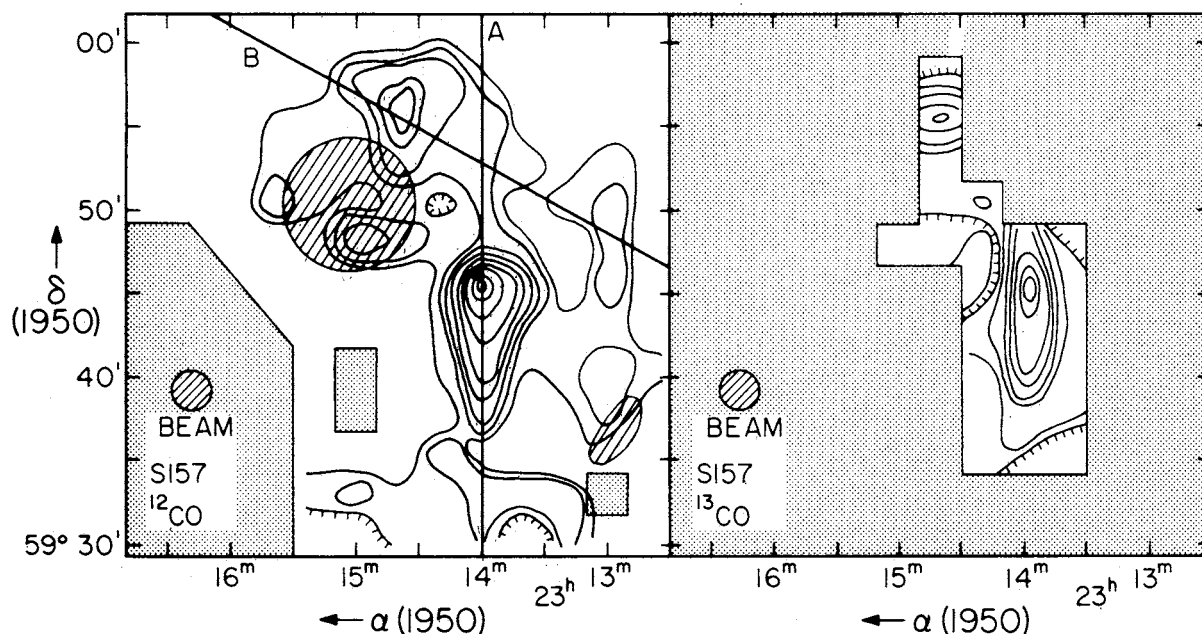


FIG. 5(a).  $^{12}\text{CO}$  and  $^{13}\text{CO}$  maps of S157, integrated over a velocity range  $V_{\text{LSR}} = -39$  to  $-51 \text{ km s}^{-1}$ . Contour values are in steps of  $6.5 \text{ K km s}^{-1}$  for  $^{12}\text{CO}$  and  $1.6 \text{ K km s}^{-1}$  for  $^{13}\text{CO}$ . In this figure and in Fig. 5(c) the H II regions discussed in the text are marked.

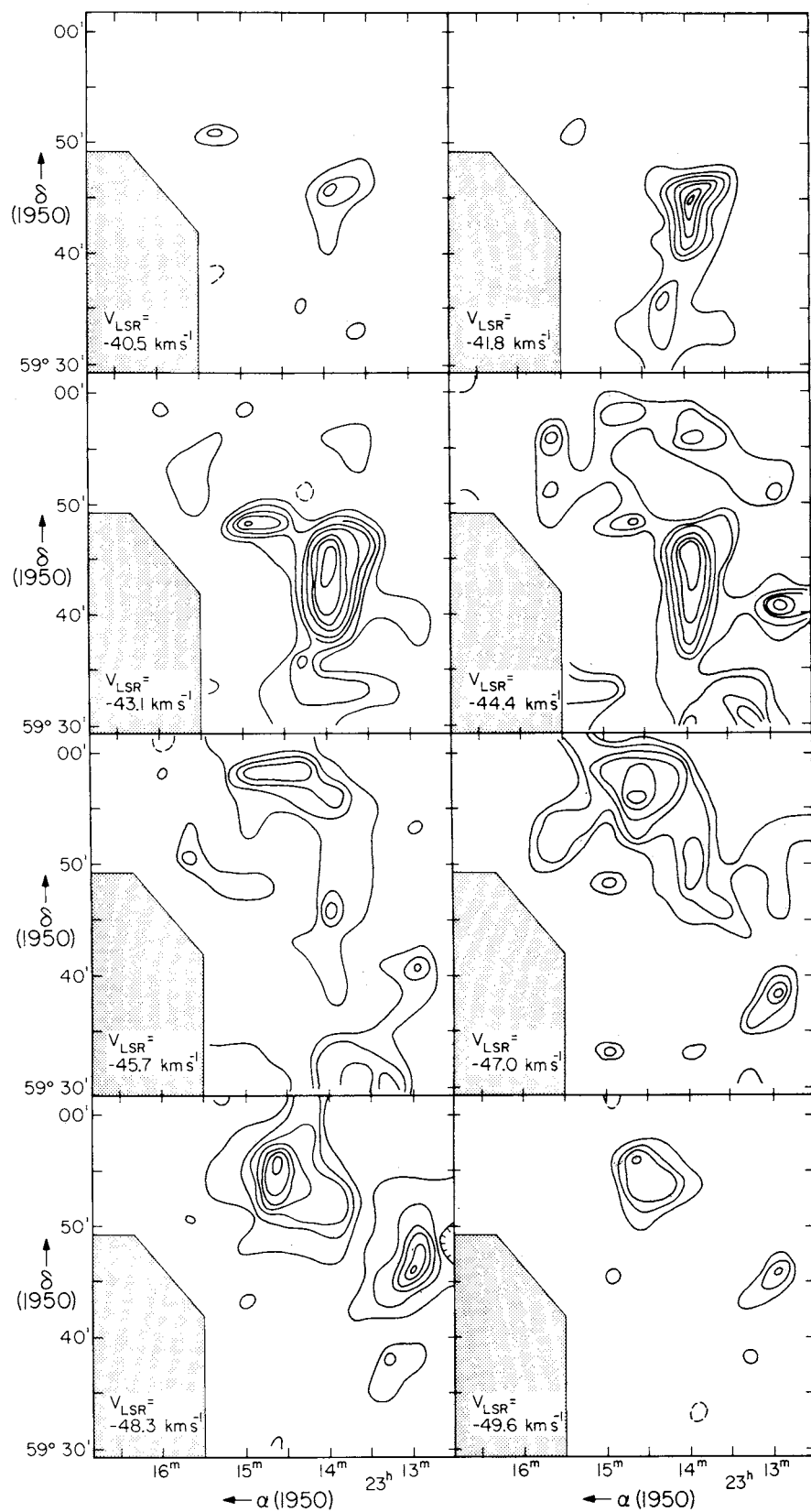


FIG. 5(b).  $^{12}\text{CO}$  channel maps, integrated over two channels. Contour values are in steps of  $1.6 \text{ K km s}^{-1}$ .

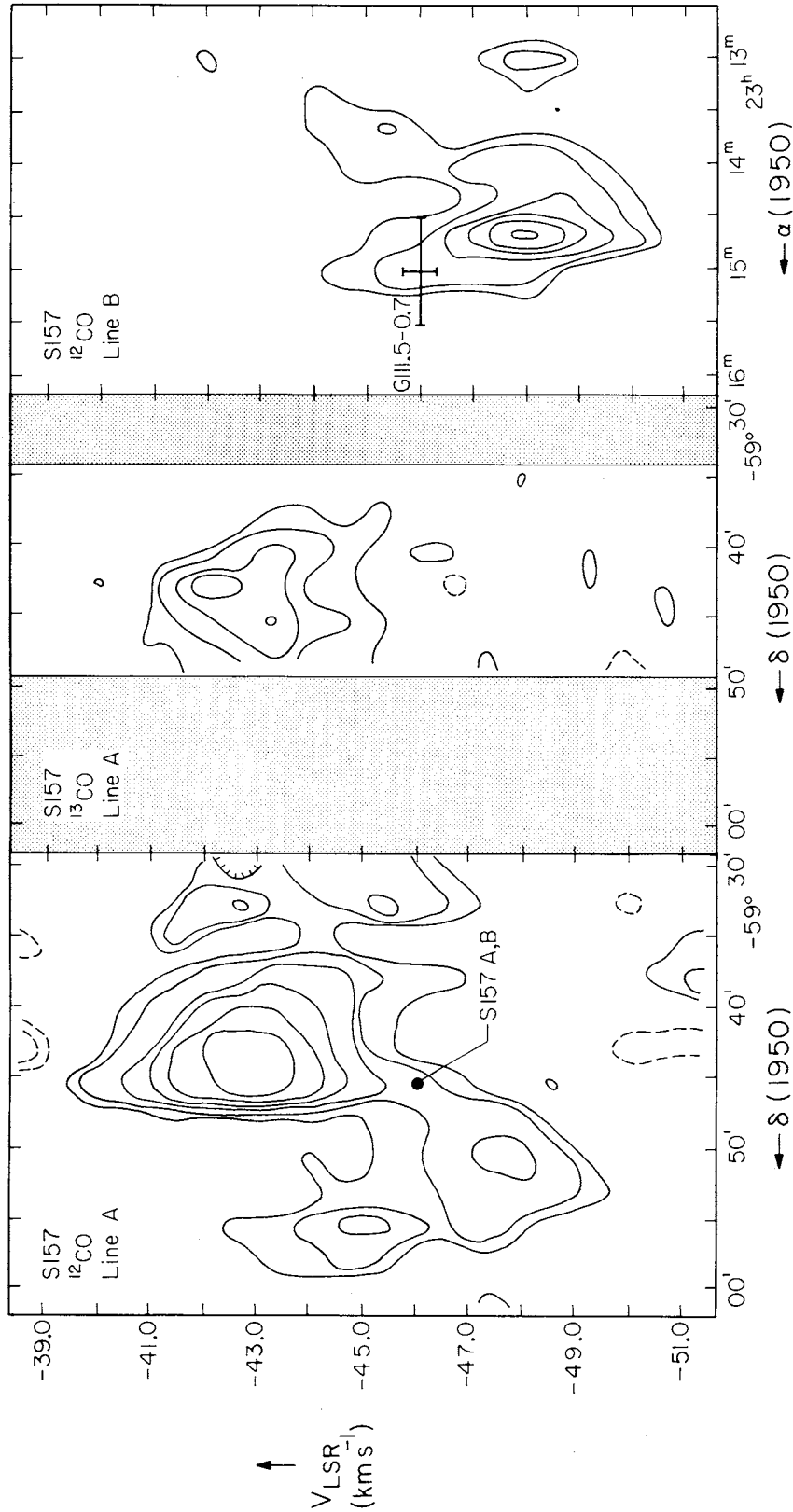


FIG. 5(c). <sup>12</sup>CO and <sup>13</sup>CO position-velocity maps along the lines marked in Fig. 5(a). Contour values are in steps of 2.5 K for <sup>12</sup>CO and 1.0 K for <sup>13</sup>CO. The 1.5-K contour is also given for the <sup>12</sup>CO maps.

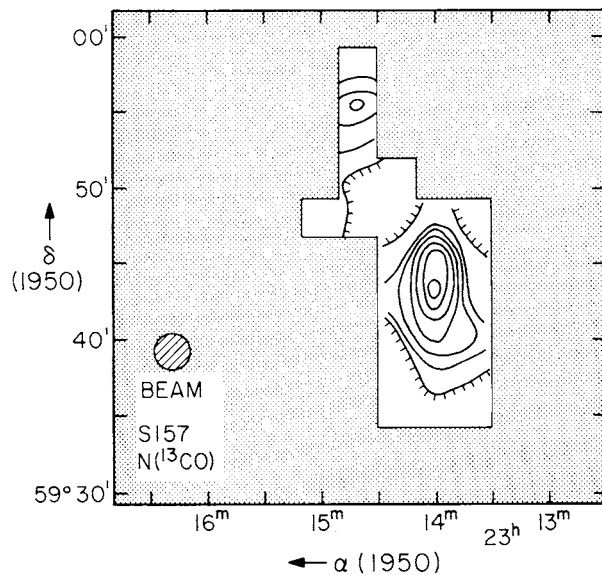


FIG. 5(d).  $^{13}\text{CO}$  column density map of S157. Contour values are in steps of  $2.5 \times 10^{15} \text{ cm}^{-2}$ .

lower-resolution data obtained with the Columbia University telescope show  $^{12}\text{CO}$  emission over an even larger range of  $23 \text{ km s}^{-1}$ , in a somewhat larger area (about one square degree).

Most remarkable are the two components CO 111.3–0.7 and CO 111.4–0.5 that were also observed in  $^{13}\text{CO}$  with the MWO telescope. The former is associated with the compact H II regions 157A and B, with  $\Delta V(\text{H}\alpha\text{--CO}) = -3 \text{ km s}^{-1}$  (Israel 1977a).

CO 111.3–0.7 has an elongated shape of  $8 \times 3 \text{ arcmin}$  ( $8 \times 3 \text{ pc}$ ); its northeastern edge is unresolved. The  $^{12}\text{CO}$  linewidth is considerably larger than the  $^{13}\text{CO}$  linewidth ( $\Delta V = 5.0 \text{ km s}^{-1}$  vs  $2.5 \text{ km s}^{-1}$ ). Although the  $^{12}\text{CO}$  and  $^{13}\text{CO}$  peaks coincide, maximum CO column densities are reached 2.5 arcmin (2.5 pc) south of the position of peak antenna temperature [Figs. 5(a) and 5(d)]; the column density map also shows an extension toward the southwest. CO 111.4–0.5 has a similar CO column density, and a similar size. Since the velocity of the H II region G111.5–0.7 is more positive than the velocity of CO 111.4–0.5 [Fig. 5(c)], it is probably associated not with it, but rather with the less dense CO 111.4–0.7 that coincides with its southern parts. This is consistent with the evolved appearance of the H II region.

Over the 30 arcmin (or 30 pc) mapped, we thus see a chain of CO clouds, at velocities different by about  $6 \text{ km s}^{-1}$ ; a typical scale for each cloud is about 5 pc. The nebula S157B is unresolved with a 6-arcsec beam (Israel 1977a). Thus the CO cloud is appreciably larger than the H II region. The ultracompact H II region S157B is located at the interface of the more extended ionized region S157A and the CO cloud 111.3–0.7. Moreover, at this position the cloud edge is unresolved by the 2.3-arcmin MWO beam. This latter fact suggests some in-

teraction between the CO cloud and S157A. It is unlikely that the formation of S157B is triggered by such an interaction, since the probable ages of S157A and B do not differ by more than a few times  $10^5 \text{ yr}$ . It is more likely that the exciting stars of both H II regions were formed by the same process at slightly different times, or with slightly different collapse times. It may be suggested that the CO cloud reaches maximum column density at some distance from the H II region/cloud interface, but the present resolution is insufficient to draw any conclusions.

#### f) S159

S159 is a compact H II region at the edge of a more extended diffuse H II region (cf. Israel 1977c). The compact component (S159A) has the appearance of a very young object, in the process of dispersing its cocoon. It has an emission measure of  $1.3 \times 10^7 \text{ pc cm}^{-6}$ , which makes it one of the brightest compact H II regions. The MWO CO maps show a very bright CO cloud [Figs. 6(a)–6(c)] roughly circular in appearance, with a diameter of 5 arcmin (5 pc) at the position of the H II region. This CO cloud seems to be part of an elongated cloud complex at least 30 pc long that contains at least two other maxima at both sides of S159, both at a distance of 10 arcmin (10 pc).

The CO column densities of the cloud associated with S159 are comparable to those of the cloud associated with S157 [see Fig. 6(d) and Table III]. There are more parallels: in the case of S159 the position of maximum column density is likewise offset from that of peak antenna temperature (by about 1.5 pc), and the compact source S159A is likewise at the interface of the more diffused ionized region S159B and the dense CO cloud. Again, the  $^{12}\text{CO}$  linewidth is about twice the  $^{13}\text{CO}$  linewidth. The eastern CO cloud CO 111.8+0.4 has a velocity that is less negative than that of CO 111.6+0.4 by  $2 \text{ km s}^{-1}$  [Figs. 6(b) and 6(c)]. This indicates the presence of a velocity gradient of  $1 \text{ km s}^{-1}$  per 10 pc for the S159 CO cloud.

To the north of S159, the edge of a more extended CO complex is seen at the slightly different velocity of  $V_{\text{LSR}} = -50 \text{ km s}^{-1}$  (rather than  $V_{\text{LSR}} = -55 \text{ km s}^{-1}$ ). This might be part of the much larger CO cloud complex that is seen immediately south of the H II region S158 (NGC 7538) (Dickel, private communication). In that case a velocity gradient of  $10 \text{ km s}^{-1}$  over about 25 pc would be implied for the S158 CO cloud.

Given the similarities between S157 and S159, the same comments that applied to the first object also apply to the second. The diffuse H II region S159B is, however, only marginally smaller than the CO cloud: 3.5 pc vs 5 pc.

#### g) S184 (NGC 281)

This is a fairly large (5-pc) evolved H II region, with

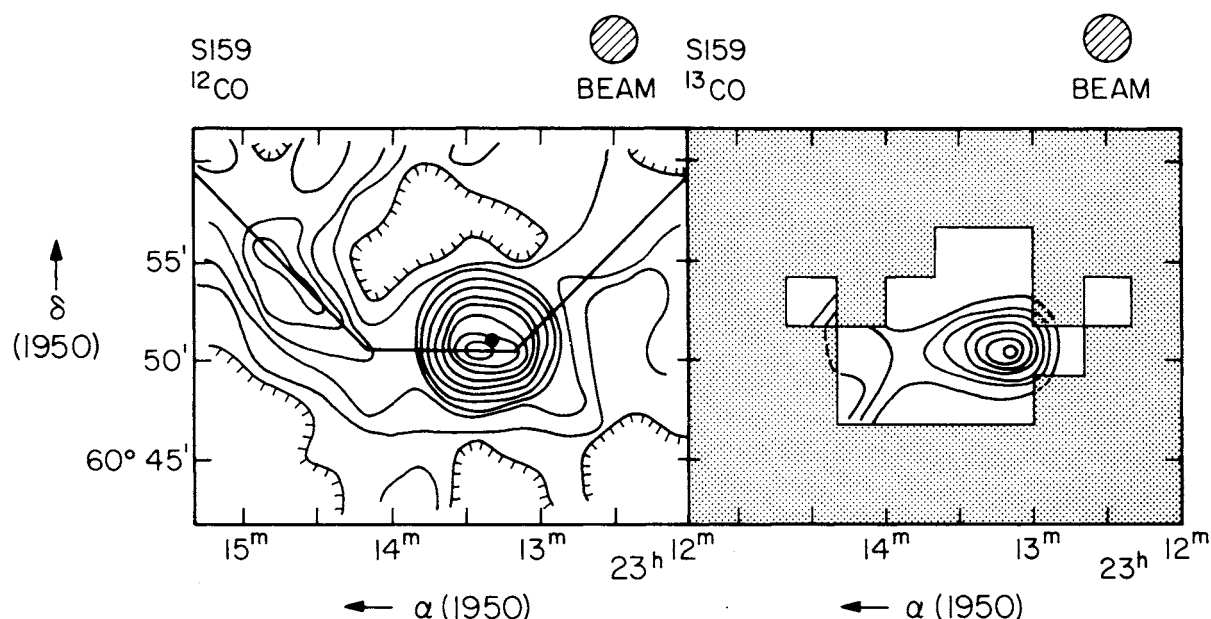


FIG. 6(a).  $^{12}\text{CO}$  and  $^{13}\text{CO}$  maps of S159, integrated over a velocity range  $V_{\text{LSR}} = -50$  to  $-63 \text{ km s}^{-1}$ . Contour values are in steps of  $6.5 \text{ K km s}^{-1}$  for  $^{12}\text{CO}$  and  $1.6 \text{ K km s}^{-1}$  for  $^{13}\text{CO}$ .  $^{13}\text{CO}$  contour of  $3.3 \text{ K km s}^{-1}$  is also given.

a radio structure indicative of two broad ionization fronts (Israel 1977b). At 8-arcmin resolution, I found an extended CO cloud of  $15 \times 35$ -arcmin ( $9 \times 20$ -pc) size. The cloud reaches maximum antenna temperatures in the northeast; this position coincides with heavy obscuration on the Palomar Sky Survey prints. Using the MWO telescope, Elmegreen and Lada (1978) found two CO clouds of sizes about 8 arcmin adjacent to the ionization-front structures seen in the radio map. They also discovered an  $\text{H}_2\text{O}$  maser at the position of one of the clouds. Elmegreen and Lada (1978) found the two clouds to have masses of  $1700M_{\odot}$  and  $260M_{\odot}$ , respectively. From the larger cloud extent I found at lower resolution, I estimate the total mass of the CO cloud associated with S184 to be of the order of  $4000M_{\odot}$ . A detailed discussion of the CO clouds and their interaction with S184 are given by Elmegreen and Lada (1978) and Elmegreen and Moran (1979).

#### h) S206 (NGC 1491)

The large evolved H II region S206 was studied in detail by Deharveng *et al.* (1976); it is a good example of an H II blister seen sidewise. It is located only 30 deg from the galactic anticenter direction, and its distance of 3.7 kpc makes it one of the outermost H II regions in the Galaxy (cf. Walmsley *et al.* 1975). It is therefore somewhat surprising, in view of the general paucity of CO clouds in the anticenter direction, to find several CO clouds in the general direction of S206 [Figs. 7(a)–7(c)].

Five clouds can be clearly identified, two of which may

be associated with S206 (Table I). On the basis of position and velocity, CO 150.5–0.8 can be considered as the parent cloud, whereas the weaker CO 150.8–1.0 farther to the south might be interacting with the expanding H II region. With  $V_{\text{LSR}} = -34.5 \text{ km s}^{-1}$  its velocity differs by almost  $10 \text{ km s}^{-1}$  from that of the H II region. The velocity difference between the H II region and the parent CO cloud is  $\Delta V(\text{H-CO}) = -2.5 \text{ km s}^{-1}$ , in accordance with the blister interpretation. The position-velocity diagram [Fig. 7(c)] in particular shows a lack of CO emission at the position of the diffuse part of the H II region.

#### i) Other H II Regions

Several other H II regions were observed, though not mapped. They are listed in Table II; the results are also shown in Fig. 8.

S188 is a filamentary nebula (Israel and Felli 1978) probably resulting from stellar mass loss and the interaction of escaping material with the interstellar medium. A weak CO cloud may be present, although one is not *a priori* expected, and there is a position offset of 10 arcmin. Near the position of the small H II region S195, a CO cloud is seen with  $V_{\text{LSR}} = -16 \text{ km s}^{-1}$ . A second, unrelated component at  $V_{\text{LSR}} = 0 \text{ km s}^{-1}$  shows up in several profiles. The CO cloud found near S196 is probably unrelated, given the large position and velocity offsets. CO emission was expected and detected near S266, S269, and S271. In the latter two cases, the (optically visible) H II region appears to be blueshifted with respect to the CO cloud, in agreement with the blister

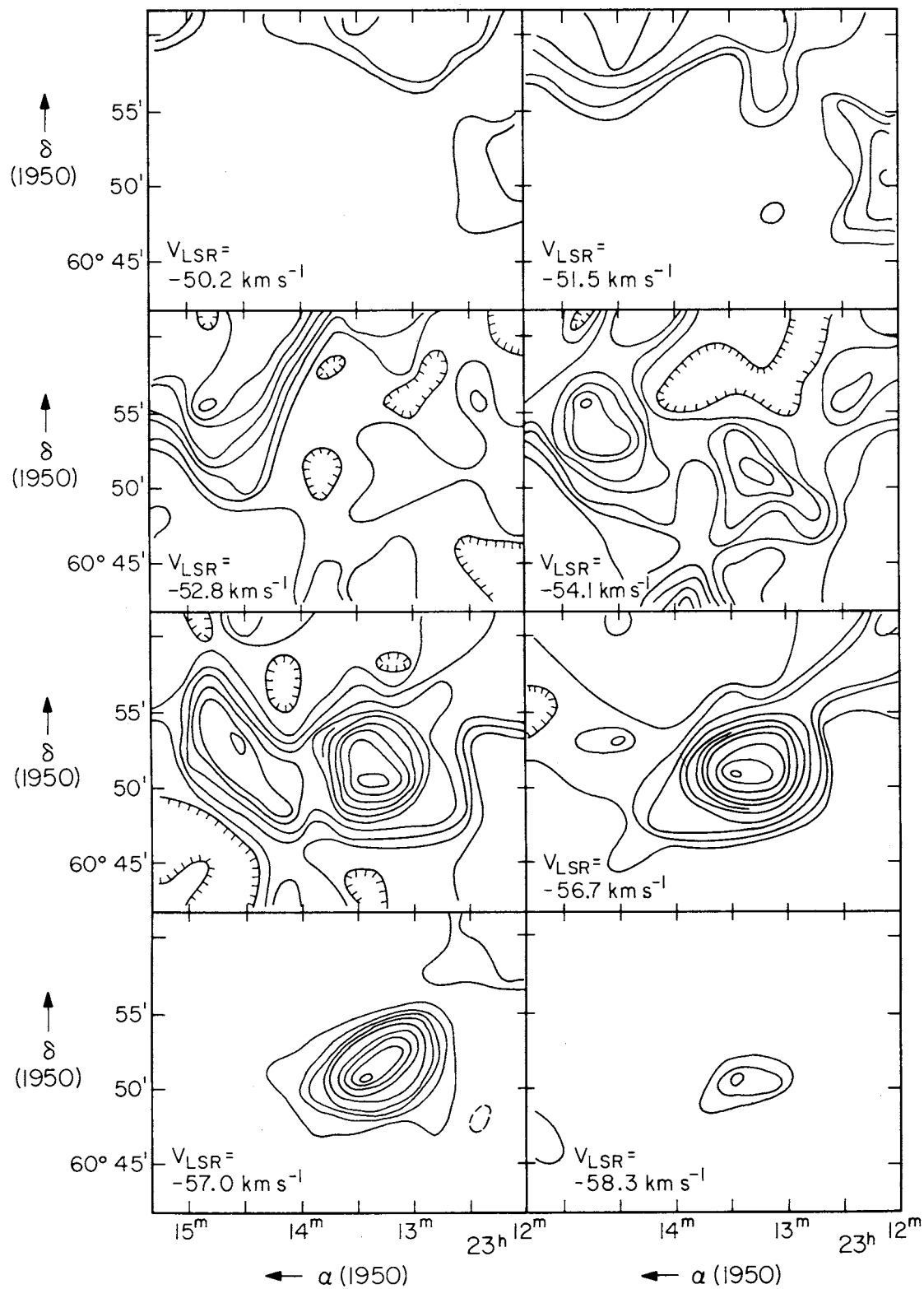


FIG. 6(b). Channel maps of  $^{12}\text{CO}$  emission integrated over two channels. Contour values are in steps of  $1.6 \text{ K km s}^{-1}$ .

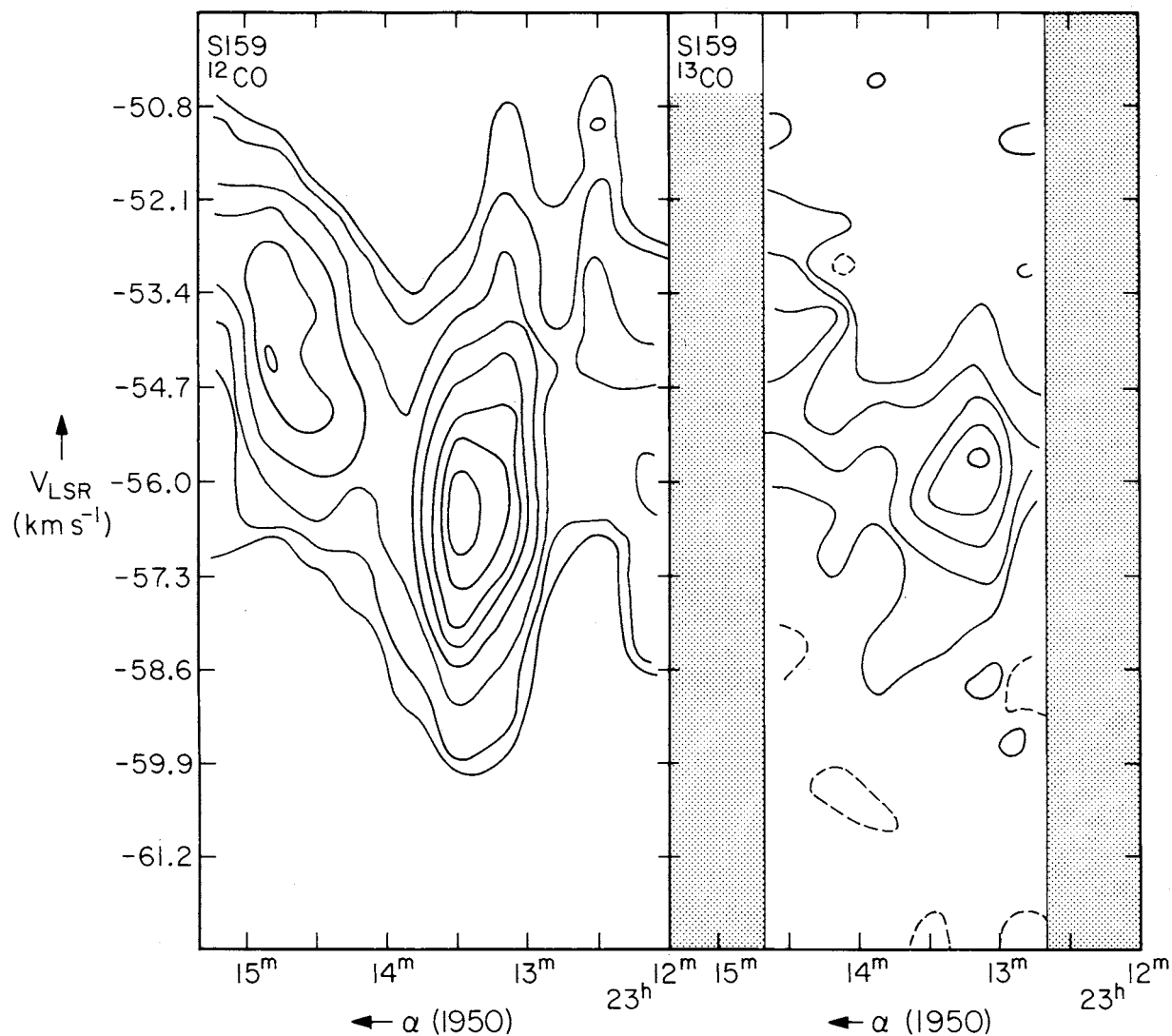


FIG. 6(c).  $^{12}\text{CO}$  and  $^{13}\text{CO}$  position-velocity maps along the line marked in Fig. 6(a). Contour values are in steps of 2.5 K for  $^{12}\text{CO}$  and 1.0 K for  $^{13}\text{CO}$ . The  $^{12}\text{CO}$  1.5-K contour is also given.

picture. Finally, in Fig. 9 I present a strip scan through the S255 cloud complex at a fixed declination. CO emission associated with the H II regions can be traced over 1.5 deg (corresponding to 50 pc at a distance of 2 kpc). The extent of the CO cloud complex associated with this H II region group, as seen with the low resolution of the Columbia University telescope, is therefore considerably larger than suggested by the MWO map (Evans *et al.* 1977), which shows emission over only 30 arcmin.

#### IV. DISCUSSION AND CONCLUSION

##### a) Star Formation in CO Clouds

In recent years several possible mechanisms for triggering star formation have been proposed. These

include galactic density waves, cloud collisions, supernova shocks, ionization shocks, and stellar winds. Each of these mechanisms has been applied to at least one source; the last two cannot initiate star formation, but are probably effective in sustaining it. From several discussions, density waves and ionization shocks have emerged as, at least for the moment, the most attractive and probably dominant mechanisms for, respectively, initiating and sustaining star formation in large complexes of molecular clouds, massive stars, and ionized regions (see, e.g., the review by Lada *et al.* 1978a).

The proposed models are all rather qualitative; this and the variety of possible mechanisms make them useful in describing the overall properties of massive aggregates of young stars and molecular clouds, but rather less so in describing detailed processes in such aggregates, or

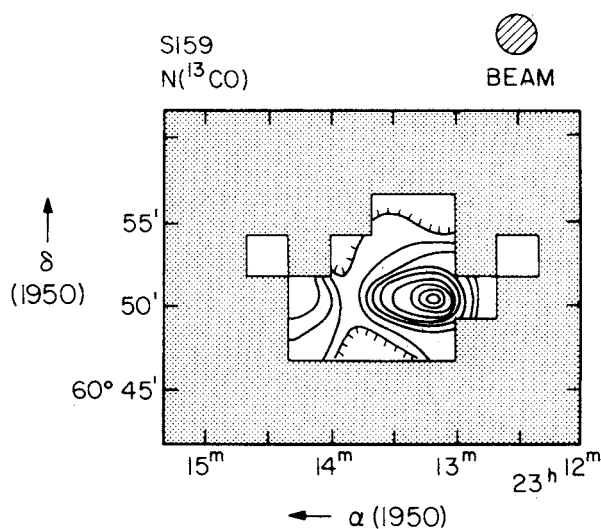


FIG. 6(d).  $^{13}\text{CO}$  column density map. Contour values are in steps of  $2.5 \times 10^{15} \text{ cm}^{-2}$ .

the properties of small H II region/molecular cloud complexes. The observations discussed in this paper are an example of this. Most of the H II regions are associated with CO clouds that only look simple when seen with sufficiently low resolution. High resolution tends to lead to rather complicated CO maps, with many distinct components at slightly different velocities. This is particularly clear in the cases of S157 and S159, and it is applied in the case of S152. Even in the case of S142 two different components are readily seen. The apparent simplicity of the S142 molecular cloud, moreover, seems to be largely a consequence of the advanced evolutionary stage of the H II region. It appears that the expansion of the H II regions has proceeded to the stage where it effectively has obliterated most of the information on density inhomogeneities that was initially present. The very large H II region S206 probably shows the same aspect; however, no high-resolution observations that might illustrate this are available. Nevertheless, even the low-resolution observations show a complicated picture, in which it is not entirely clear in what manner the expanding H II region interacts with its surroundings.

A second aspect should be mentioned here. From previous work (Israel 1976c; Habing and Israel 1979), it has become clear that compact H II regions are with very few exceptions always found in groups near other H II regions rather than isolated. To a somewhat lesser degree this also holds true for more expanded H II regions. Examples among the H II regions discussed in this paper are S157A and B and S159A and B. The CO observations of these objects described above, and those of S158 (Dickel, private communication), show that the obscured compact H II regions are located at the edge of fairly compact CO clouds, roughly where a more expanded and less dense H II region touches the CO cloud. Once again there is no unique explanation at this mo-

ment. Because of the time scales and distance scales involved (typically a few times  $10^5$  yr and 1–2 pc), the sequential star-formation model of Elmegreen and Lada (1977) cannot be applied. But it is possible that the shock due to the expanding H II region has triggered the collapse of a massive globule that was already present, and “primed” for star formation. On the other hand, it is equally possible that both the compact and the expanded H II regions are due to stars that were triggered by the same mechanism, at slightly different times or with slightly different collapse times.

#### b) Masses of Neutral and Ionized Material

Another problem is that of the role of CO clouds vs H I clouds. Several cases are now known where both are present: they include S125 (IC 5146), S184 (NGC 281) (Riegel 1967; this paper), W58 (K3-50 complex) (see Israel 1980), S158, and S159 (Read, in preparation), while in many cases (for instance, S206 and the S147/S153 group) CO clouds are located close in space and velocity to large H I complexes seen in galactic H I surveys. For S158, S159, and W58, high-resolution H I observations are now available, thanks to Read’s aperture synthesis observations with the Cambridge Half-Mile Telescope. In these sources a small CO cloud ( $d \leq 5$  pc) appears to form the interface between the ionized regions and neutral hydrogen regions, and might possibly be identified with the postshock layer described by Elmegreen and Lada (1977) in their model of sequential star formation. But it is not clear whether this is indeed the case, in particular in view of the time scales involved. Star-formation processes have typical time scales of  $10^5$ – $10^6$  yr, whereas typical time scales for the conversion of H to  $\text{H}_2$ , or C and O to CO are thought to be in excess of  $10^7$  yr. On the other hand, studies of giant molecular complexes (Blitz and Shu 1980; Larson 1980) indicate lifetimes of the order of  $10^7$  yr, implying time scales

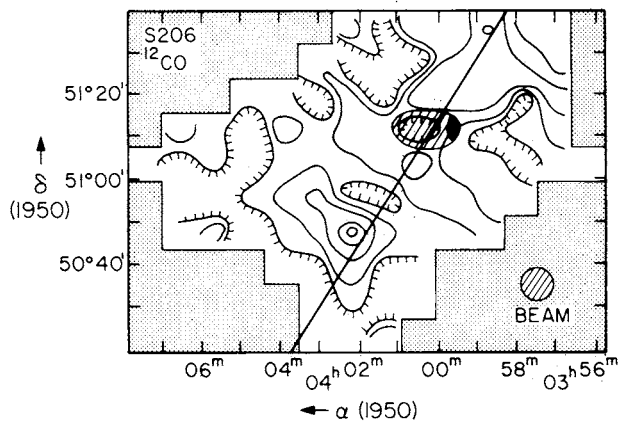


FIG. 7(a).  $^{12}\text{CO}$  map of S206. The extent of the densest part of the H II region is marked. The map is integrated over a velocity range  $V_{\text{LSR}} = +3$  to  $-56 \text{ km s}^{-1}$ . Contour values are in steps of  $6.5 \text{ K km s}^{-1}$ .

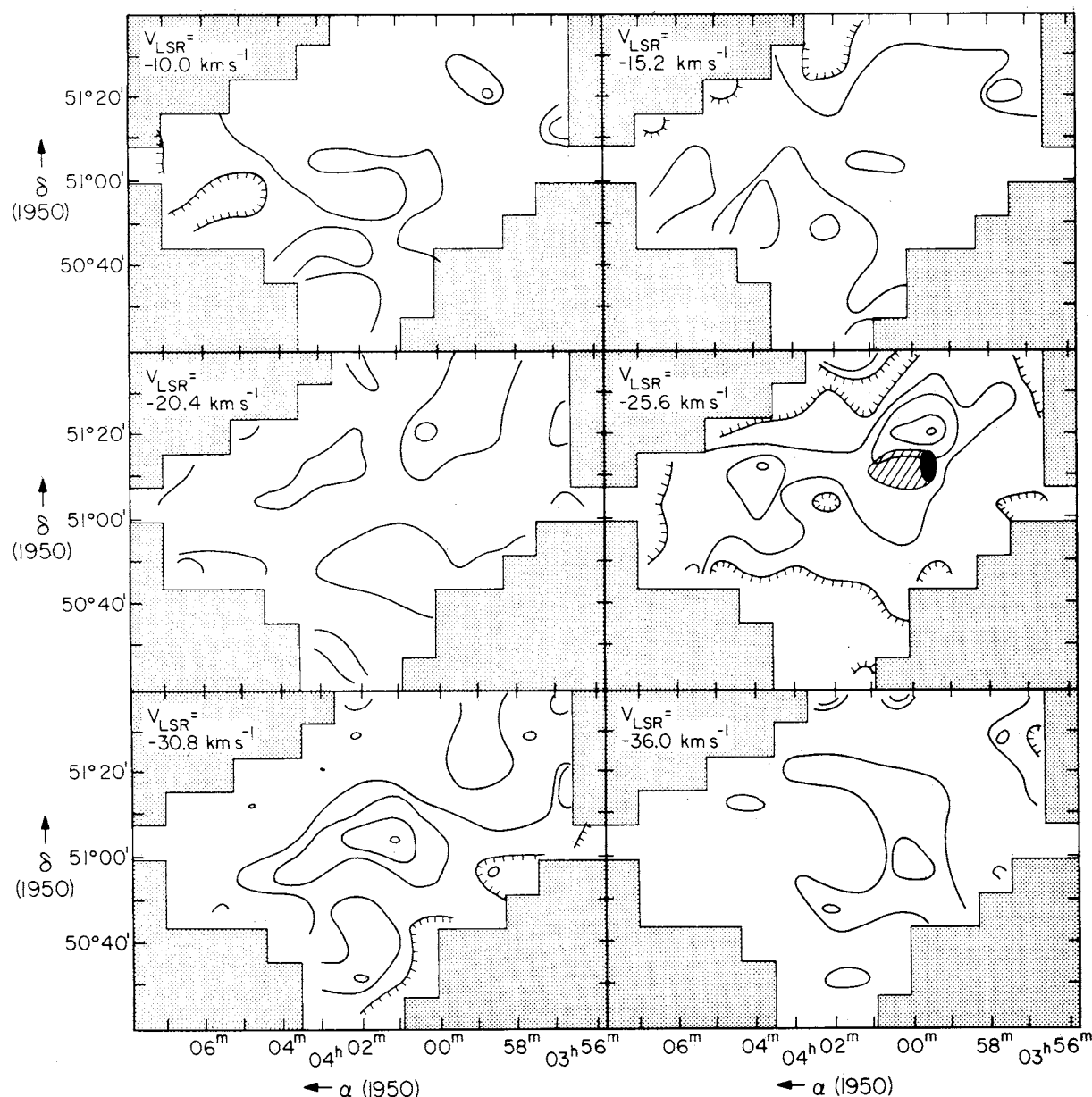


FIG. 7(b). Channel maps of  $^{12}\text{CO}$  emission integrated over two channels. Contour values are in steps of  $2.6 \text{ K km s}^{-1}$ .

$\lesssim 10^7$  yr for the conversion of atomic to molecular gas. If conversion times can be made sufficiently short—at most, of the order of  $10^6$  yr—at least part of the observed CO might be formed *after* star-formation processes were initiated in the cloud complex. If this is not the case, the neutral hydrogen clouds associated with the CO complexes must be considered as material left over in the compression process that originally created the giant molecular clouds (cf. Blitz and Shu 1980). Under those circumstances it is not clear what fraction of the H I cloud complex that is seen in the low-resolution surveys is directly involved in the star-formation process, if any at all.

A comparison of the masses involved, in the form of stars, ionized clouds, and neutral clouds, is given in Table IV. Each of the masses tabulated is subject to considerable uncertainty, but a comparison nevertheless yields interesting results.

The stellar masses are all calculated on the basis of a Salpeter-type initial mass function, truncated at spectral type K5; the upper limit for the integration was determined from the total excitation parameters of the associated ionized regions that provide an estimate for the most luminous star present. For an individual region the total stellar mass is uncertain by a factor of 2. However, if low-mass stars do not form together with high-mass

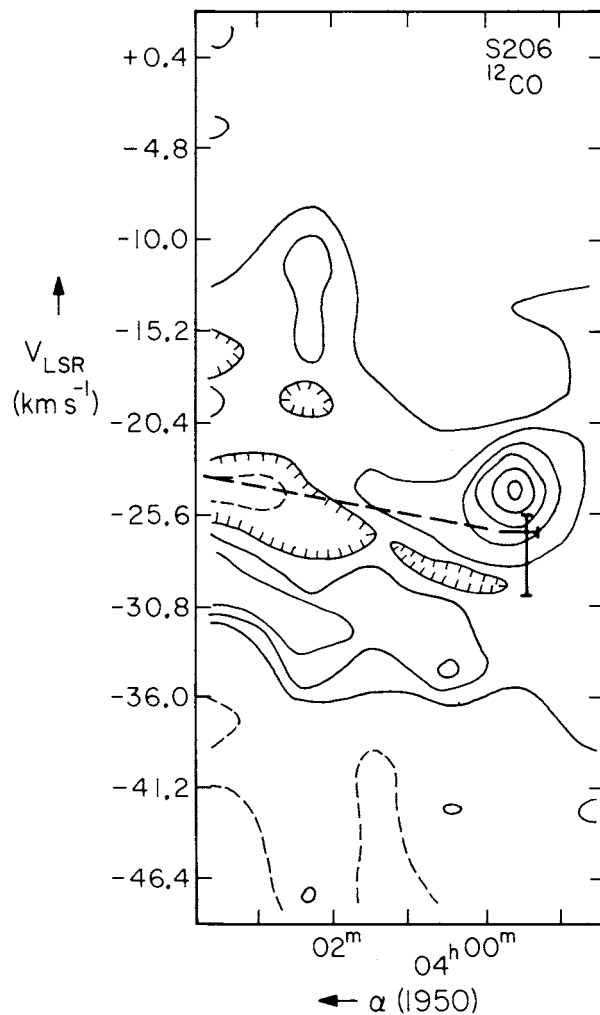


FIG. 7(c). Position-velocity map in  $^{12}\text{CO}$  along the line marked in Fig. 7(a). The position of the extended H II region is also indicated. Contour values are in steps of 0.5 K. The dotted line indicates the extent of the large, diffuse H II region envelope.

stars, the estimate may be too high by a factor of 5. The ionized masses are largely determined from aperture synthesis radio observations, assuming no clumping. They are therefore upper limits. However, if a low surface brightness envelope is present, this may increase the mass considerably: for S252 I listed both the mass present in the form of relatively small components, and the total mass derived from low-resolution, single dish observations. The neutral mass is calculated from  $^{12}\text{CO}$  and  $^{13}\text{CO}$  observations, and is subject to the usual uncertainties. On the whole, I expect that the order of magnitude is correct for all but one or two sources. The complicating role of neutral hydrogen is illustrated by the cases of S125 and S142: Riegel's (1967) observations yield an H I mass of two-thirds the  $\text{H}_2$  mass for S125, but four times the  $\text{H}_2$  mass for S184. Again it is not known whether this mass plays any role in the process of star formation at this location. From Table IV, it appears that

the stellar mass of the small H II regions, or small H II region groups, varies by only a factor of 2. In the large H II regions and large H II region complexes, it is on the average higher by a factor of 3 to 6. The ionized masses vary strongly; the highest are found for the most evolved H II regions (S142, S252), which is to be expected from simple considerations regarding the evolution of H II

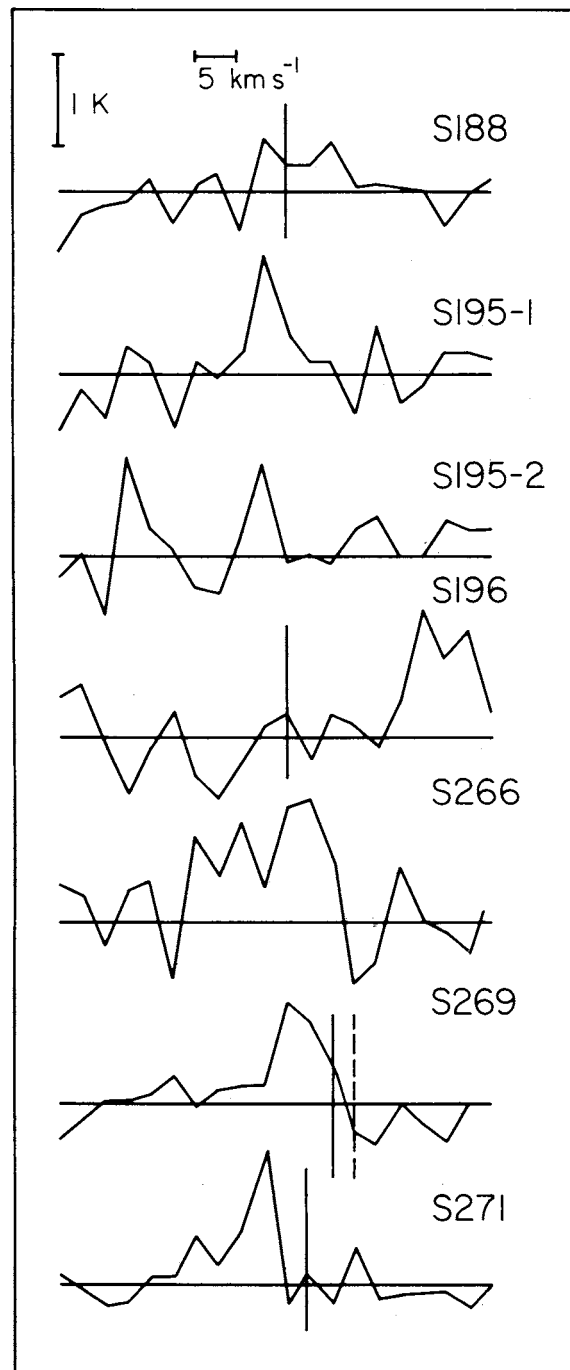


FIG. 8.  $^{12}\text{CO}$  scans through several H II regions. Positions are given in Table II.

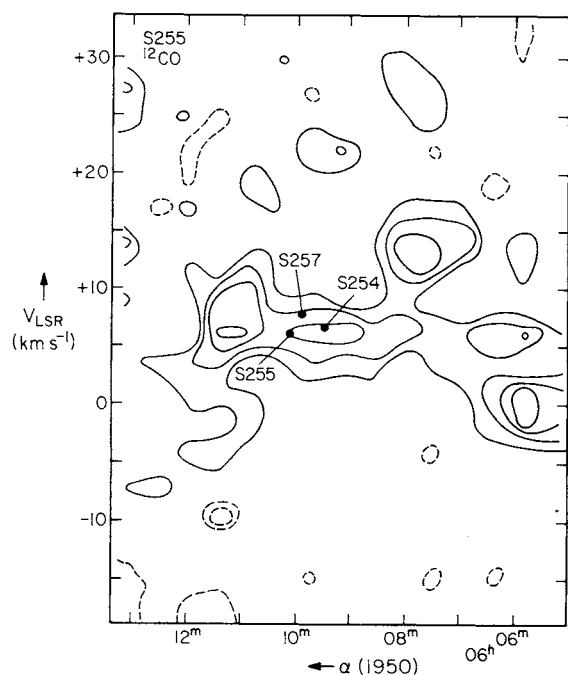


FIG. 9. Position-velocity map in  $^{12}\text{CO}$  of the S255 (IC 2162) H II region complex at constant declination (Decl. =  $18^\circ 02'$ ). Contour values are 0.5 K.

regions. The data in Table IV indicate that on scales less than 10 pc the star-formation process is quite efficient: 30–50% of the total mass is in the form of stars. For the larger regions the stellar contribution to the total mass

drops to a few percent, in accordance with present-day estimates of the overall efficiency of star-formation processes in molecular cloud complexes.

The  $\text{H}_2$  masses calculated from the CO observations likewise show a large variation, but here the highest masses are found near the H II regions that are least evolved (the K3-50 complex near S100, S106). In particular, the ratio  $M(\text{H}_2)/M(\text{H II})$  varies strongly, from values of 500–1000 (S106, K3-50 complex, W3) down to values as low as 0.1 (S142). It thus appears that the evolutionary stage of an H II region–molecular cloud complex is strongly correlated with the fraction of hydrogen present in ionized form. This conclusion is somewhat tentative, however, because of the observational uncertainties.

At present it is not obvious what causes the declining role of dense neutral clouds containing CO and  $\text{H}_2$ . On the one hand, it may indicate the erosion of the dense parent cloud by the expanding H II region. On the other hand, it may be due to the weakening or disappearance of the star-formation trigger: no more neutral material is compressed to high densities and the existing high-density clouds may evaporate or disperse.

In order to make further progress on the above problems, more high-resolution observations are necessary, in particular aperture synthesis H I observations at about 1-arcmin resolution and CO observations with resolutions of about 15 arcsec of bright rims and CO cloud/H II region interfaces. From the theoretical side, more detailed models of the collapse and fragmentation of dense clouds are desirable.

TABLE IV. Comparison of masses.

Object	Stellar $M(\text{stars})$	Ionized $M(\text{H II})$	Neutral $M(\text{H}_2)$	Ratio $M(\text{H}_2)/M(\text{H II})$	References
S99	750	32	2400	75	1, 2
S106	670	50	54000	1080	3, 4
S125 (IC 5146) <sup>a</sup>	470	7	1000	145 ( )	5, 6
S142 (NGC 7380) <sup>b</sup>	530	2000	200	0.1	5, 6
S157A+B	470	10	800	80	7, 6
S159A+B	815	70	750	11	7, 6
S184 (NGC 281) <sup>c</sup>	815	130	4000	31 (154)	5, 8
S228	470	30	2000	67	5, 9
S255 complex	470	35	5000	145	10, 11
S100 (K3-50 complex)	1930	250	110000	440	1, 2
S252 (NGC 2175)	1890	5200 (100)	25000	5 (250)	12, 13
W3	1350	20	12000	600	14, 15
M17	4300	550	120000	200	16, 17

<sup>a</sup>  $M(\text{stars}) = 250M_\odot$ ;  $M(\text{H I}) = 670M_\odot$  (Riegel 1967).

<sup>b</sup>  $M(\text{stars}) = 440M_\odot$ ;  $M(\text{dust}) = 50M_\odot$  (Moffat 1971).

<sup>c</sup>  $M(\text{H I}) = 16000M_\odot$  (Riegel 1967).

Reference list for Table IV

1. Israel (1976a).
2. Israel (1980).
3. Israel and Felli (1978).
4. Lucas *et al.* (1978).
5. Israel (1977b).
6. This paper.
7. Israel (1977a).
8. Elmegreen and Lada (1978).
9. Lucas and Erenenz (1975).
10. Israel (1976b).
11. Evans *et al.* (1977).
12. Felli *et al.* (1977).
13. Lada and Wooden (1979).
14. Wynn-Williams (1971).
15. Dickel (1979).
16. Lemke (1975).
17. Elmegreen *et al.* (1979).

These observations would have been impossible without the encouragement and hospitality of Pat Thaddeus at the Goddard Institute of Space Studies in New York. I also thank Leo Blitz, George Tomasevich, Richard Cohen, and Hong-ih Cong for their continuous

advice and assistance in obtaining the observations. Part of this work was done while I was at the Observatory at Leiden; research at the Owens Valley Radio Observatory is supported by NSF Grant AST 077-00247.

## REFERENCES

- Bally, J., and Scoville, N. Z. (1980). Preprint.
- Baran, G. (1978). Ph.D. thesis, Columbia University.
- Bergeat, J., Sibille, F., and Lunel, M. (1975). *Astron. Astrophys.* **40**, 347.
- Blair, G. N., Evans, N. J., Vanden Bout, P. A., and Peters, W. L. (1978). *Astrophys. J.* **219**, 896.
- Blair, G. N., Peters, W. L., and Vanden Bout, P. A. (1975). *Astrophys. Lett.* **200**, L161.
- Blitz, L. Private communication.
- Blitz, L., and Shu, F. H. (1980). *Astrophys. J.* **238**, 148.
- Cong, H.-I. (1977). Ph.D. thesis, Columbia University.
- Davis, J. H., and VandenBout, P. (1973). *Astrophys. Lett.* **15**, 43.
- Deharveng, L., Israel, F. P., and Maucheret, M. (1976). *Astron. Astrophys.* **49**, 63.
- Dickel, H. R. Private communication.
- Dickel, H. R. (1979). *Astron. Astrophys.* (in press).
- Dickel, H. R., Dickel, J. R., Wilson, W. J., and Werner, M. W. (1980). *Astrophys. J.* **237**, 711.
- Dickel, J. R., Dickel, H. R., and Wilson, W. J. (1978). *Astrophys. J.* **223**, 840.
- Dickinson, D. F., Frogel, J. A., and Persson, S. E. (1974). *Astrophys. J.* **192**, 347.
- Dickman, R. L. (1978). *Astrophys. J. Suppl.* **37**, 407.
- Elias, J. H. (1978). *Astrophys. J.* **223**, 859.
- Elmegreen, B. G., and Lada, C. J. (1977). *Astrophys. J.* **214**, 725.
- Elmegreen, B. G., and Lada, C. J. (1978). *Astrophys. J.* **219**, 467.
- Elmegreen, B. G., and Moran, J. M. (1979). *Astrophys. J. Lett.* **227**, L93.
- Elmegreen, B. G., Lada, C. J., and Dickinson, D. F. (1979). *Astrophys. J.* **230**, 415.
- Evans, N. J., Blair, G. N., and Beckwith, S. (1977). *Astrophys. J.* **217**, 448.
- Felli, M., Habing, H. J., and Israel, F. P. (1977). *Astron. Astrophys.* **59**, 43.
- Felli, M., Harten, R. H., Habing, H. J., and Israel, F. P. (1978). *Astron. Astrophys. Suppl.* **32**, 423.
- Frogel, J. A., and Persson, S. E. (1972). *Astrophys. J.* **178**, 667.
- Georgelin, Y. M. (1975). Ph.D. thesis, Université de Provence, Marseilles, France.
- Habing, H. J., and Israel, F. P. (1979). *Annu. Rev. Astron. Astrophys.* **17**, 345.
- Israel, F. P. (1976a). *Astron. Astrophys.* **48**, 193.
- Israel, F. P. (1976b). *Astron. Astrophys.* **52**, 175.
- Israel, F. P. (1976c). Ph.D. thesis, Leiden University.
- Israel, F. P. (1977a). *Astron. Astrophys.* **59**, 27.
- Israel, F. P. (1977b). *Astron. Astrophys.* **60**, 233.
- Israel, F. P. (1977c). *Astron. Astrophys.* **61**, 372.
- Israel, F. P. (1978). *Astron. Astrophys.* **70**, 769.
- Israel, F. P. (1980). *Astrophys. J.* **236**, 465.
- Israel, F. P., and Felli, M. (1978). *Astron. Astrophys.* **63**, 325.
- Israel, F. P., Habing, H. J., and deJong, T. (1973). *Astron. Astrophys.* **27**, 143.
- Lada, C. J. (1976). *Astrophys. J. Suppl.* **32**, 603.
- Lada, C. J., Blitz, L., and Elmegreen, B. G. (1978a). In *Protostars and Planets*, edited by T. Gehrels (University of Arizona, Tucson), p. 341.
- Lada, C. J., and Elmegreen, B. G. (1979). *Astron. J.* **84**, 336.
- Lada, C. J., Elmegreen, B. G., Cong, H.-I., and Thaddeus, P. (1978b). *Astrophys. J. Lett.* **226**, L39.
- Lada, C. J., and Wooden, D. (1979). *Astrophys. J.* **232**, 158.
- Larson, R. B. (1980). Preprint.
- Lemke, D. (1975). In *H II Regions and Related Topics*, edited by T. L. Wilson and D. Downes [Springer, Heidelberg (BRD)], p. 372.
- Liszt, H. S. (1973). Ph.D. thesis, Princeton University.
- Lo, K. Y., Burke, B. F., and Haschick, A. D. (1975). *Astrophys. J.* **202**, 81.
- Lucas, R., and Encrenaz, P. J. (1975). *Astron. Astrophys.* **41**, 233.
- Lucas, R., Le Squérèn, A. M., Kazès, I., and Encrenaz, P. J. (1978). *Astron. Astrophys.* **66**, 155.
- Milman, A. S., Knapp, G. R., Knapp, S. L., and Wilson, W. J. (1975). *Astron. J.* **80**, 101.
- Moffat, A. R. J. (1971). *Astron. Astrophys.* **13**, 30.
- Mufson, S. L., and Liszt, M. S. (1977). *Astrophys. J.* **212**, 664.
- Nadeau, D. Private communication.
- Price, S. D., and Walker, R. C. (1976). "The AFGL Four Color Infrared Sky Survey," Report No. AFGL-TR-76-0208, Hanscomb AFB, Massachusetts.
- Read, X. In preparation.
- Riegel, K. W. (1967). *Astrophys. J.* **148**, 87.
- Sharpless, S. (1959). *Astrophys. J. Suppl.* **4**, 257.
- Walker, M. F. (1959). *Astrophys. J.* **130**, 57.
- Walmsley, C. M., Churchwell, E., Kazès, I., and Le Squérèn, A. M. (1975). *Astron. Astrophys.* **41**, 121.
- Westerhout, G. (1969). *Maryland-Green Bank Galactic 21 cm Line Survey*, 2nd ed. (University of Maryland, College Park, Maryland).
- Wilson, W. J., Schwartz, P. R., Epstein, E. E., Johnson, W. A., Etcheverry, R. D., Mori, T. T., Berry, C. G., and Dyson, H. B. (1974). *Astrophys. J.* **191**, 357.
- Wynn-Williams, C. G. (1971). *Mon. Not. R. Astron. Soc.* **151**, 397.